Direct Control of a Passive Haptic Device Based on Passive Force Manipulability Ellipsoid Analysis

Changhyun Cho, Munsang Kim, and Jae-Bok Song

Abstract: In displaying a virtual wall using a passive haptic device equipped with passive actuators such as electric brakes, unsmooth motion frequently occurs. This undesirable behavior is attributed to time delay due to slowness in the virtual environment update and force approximation due to the inability of a brake to generate torque in arbitrary directions. In this paper a new control scheme called direct control is proposed to achieve smooth display on the wall-following task with a passive haptic device. In direct control, brakes are controlled so that the normal component of a resultant force at the end-effector vanishes, based on the force analysis at the end-effector of the passive haptic device using the passive FME (Force Manipulability Ellipsoid). Various experiments have been conducted to verify the validity of the direct control scheme with a 2-link passive haptic system.

Keywords: FME, Force approximation, haptics, passive haptic devices, unsmooth motion.

1. INTRODUCTION

Compared with an active actuator, a passive actuator such as a brake is stable and has the advantage of a good torque/mass ratio. Furthermore, its relatively small energy consumption makes it suitable for portable devices. Since most real or virtual environments can be modeled as passive systems, use of passive actuators for haptic devices can be justified. Taking these benefits into account, haptic devices equipped with passive actuators can be a good solution to portable or wearable haptic devices.

The most serious drawback of passive haptic devices is that a passive actuator can generate torque only against its motion. This feature may be beneficial in terms of stability, but it often leads to poor performance in haptic display in that the passive actuator is not able to generate torque in an arbitrary direction. On the wall-following task of multi-DOF passive haptic systems, unsmooth motion (e.g., repeated contact and non-contact of the end-effector with the virtual wall) is often observed. This phenomenon is caused by force approximation due to passive actuators incapable of generating torque in arbitrary directions [1]. Several control algorithms have been suggested to avoid this unsmooth motion display as follows.

Book et al. presented a planar haptic device based on the 5-bar mechanism equipped with four brakes for the 2 DOF haptic display [2]. This redundancy in actuation increased the haptic performance of the device. As a successive research, Swanson and Book presented a single DOF controller (SDOF Controller), which used a SDOF line achieved by locking one brake to reduce a system's DOFs and achieve smooth display [3]. The proposed SDOF controller was shown to be simpler and more effective than the velocity controller presented by Davis and Book [4]. To avoid unsmooth force display, they also presented optimal control on the velocity ratio controller [5], where cost functions were used to minimize approximation angle and kinetic energy loss. However, a velocity field should be determined prior to displaying a desired path.

Sakaguchi et al. presented a passive haptic device with a 5 bar mechanism and two ER (Electro-Rheological) brakes [6]. To move along the surface of a virtual wall, a small band was established near the surface. Only one brake was activated in the small band as in the SDOF controller of [3]. However, the proposed method for moving along the surface could disturb motion toward the free space.

To avoid unsmooth force display, the most previous research employed special control methods (e.g., construction of a band or a velocity field) in which wall-contact is inconsistent with wall-following. For an active haptic device, however, the identical control

Manuscript received October 14, 2003; revised March 29, 2004; accepted April 2, 2004. Recommended by Editorial Board member Won-jong Kim under the direction of Editor Shuzhi Sam Ge.

Changhyun Cho is with the Dept. of Mechanical Eng. at Korea University and the Intelligent Robotics Research Center at KIST, 39-1, Hawolgok-dong, Seongbuk-gu, Seoul, 136-791, Korea (e-mail: chcho@kist.re.kr).

Munsang Kim is with the Intelligent Robotics Research Center at KIST, 39-1, Hawolgok-dong, Seongbuk-gu, Seoul, 136-791, Korea (e-mail: munsang@kist.re.kr).

Jae-Bok Song is with the Dept. of Mechanical Eng. at Korea University, Anam-dong, Seongbuk-gu, Seoul, 136-701, Korea (e-mail: jbsong@korea.ac.kr).

scheme can be used for both wall-contact and wall-following tasks. That is, the active haptic device just displays the force required to prevent penetration into the virtual wall for both tasks and no special scheme is necessary for smooth movement in the wall-following task. This control scheme in active haptic devices is generally accepted in the haptic community, so it is preferable that a similar control scheme should be applied to passive haptic systems.

In this paper, a new control method for a passive haptic system is proposed, which is consistently applicable to both wall-contact and wall-following tasks while avoiding unsmooth force display in the wall-following task. In order to understand force approximation in a passive haptic device, the passive FME (Force Manipulability Ellipsoid) analysis proposed by Cho et al. will be used as an analytical tool [7]. The passive FME is a constrained FME, which graphically illustrates the mapping between a torque in joint space and a force in task space [8]. It can be found from this analysis that unsmooth display may occur when force approximation is made with time delay. Since the force distribution at the end-effector can be readily available in the passive FME, we can design a new control scheme that sets the normal component of a resultant force at the end-effector to zero. With the proposed control scheme, we can achieve smooth display on the wall-following task.

The balance of this paper is organized as follows. The passive FME is briefly introduced in Section 2, and unstable behavior of a passive haptic device is discussed in Section 3. A new force control scheme is proposed in Section 4. Section 5 deals with the 2 DOF coupled tendon-drive mechanism, which was developed for experimental verification of the proposed control scheme and shows some experimental results. Conclusions are drawn and future work is outlined in Section 6.

2. PASSIVE FME

To investigate limitations of a passive haptic device, consider the Jacobian mapping between the joint torques in joint space and the end-effector forces in task space as shown in Fig. 1. The inner product of the torque vector and the angular velocity vector for the n DOF mechanism is given by

$$\tau \cdot \dot{\mathbf{q}} = \sum_{i=1}^{n} \tau_i \cdot \dot{q}_i . \tag{1}$$

The joint space can be divided into the active region where $\tau \cdot \dot{\mathbf{q}} > 0$ and the passive region where $\tau \cdot \dot{\mathbf{q}} \le 0$. The passive region is further divided into passive region I in which all joints are passive (i.e., $\tau_i \cdot \dot{q}_i \le 0$ for all i) and passive region II in which some joints are active (i.e., $\tau_i \cdot \dot{q}_i > 0$ for some i) while $\tau \cdot \dot{\mathbf{q}} \le 0$ still holds. Note that the torque generated by a motor satisfies either $\tau_i \cdot \dot{q}_i \le 0$ or $\tau_i \cdot \dot{q}_i > 0$, but the torque generated by a brake satisfies only $\tau_i \cdot \dot{q}_i \le 0$. Passive region I in the joint space is mapped into the corresponding passive region I in the task space, but its distribution or shape in the task space cannot be easily estimated from the information on the joint space. In what follows, a method for representing passive region I in the task space will be described by the Jacobian mapping:

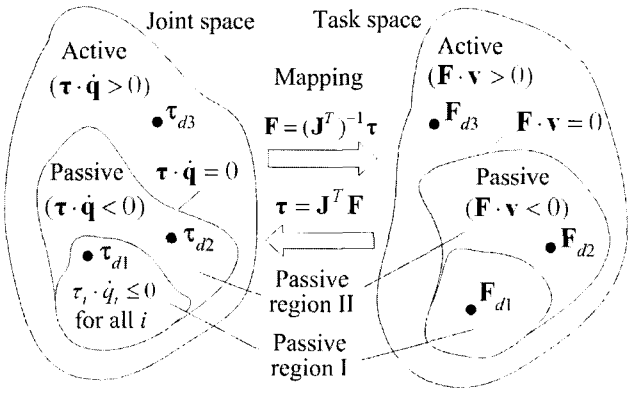

Fig. 1. Mapping between joint and task spaces.

$$\tau = \mathbf{J}(\mathbf{q})^T \mathbf{F}, \tag{2}$$

where $\mathbf{J}$ is the manipulator Jacobian matrix, $\mathbf{q}$ is the n-dimensional joint variable vector, and $\mathbf{F}$ is the m-dimensional end-effector force vector, respectively. To simplify the problem, we assume that $m = n$ so that the Jacobian matrix is invertible. A so-called force manipulability ellipsoid (FME) can be drawn from (2) by finding a set of all end-effector forces that are realizable by a joint torque vector whose Euclidean norm satisfies the condition $\| \tau \| = (\tau_1^2 + \cdots + \tau_n^2)^{1/2} \le 1$.

The forces available at the end-effector (i.e., passive region I in task space) can be computed from the torques generated by brakes (i.e., passive region I in the joint space). A brake torque is determined depending on how the brake is controlled. In an electric brake, for instance, only the magnitude of the brake torque can be controlled, since changing the polarity of the electromagnet does not affect the direction of a braking torque. A brake can generate its braking torque so that $\tau_i \cdot \dot{q}_i \le 0$ is satisfied. Therefore, if the brake is commanded to generate a desired torque τ_d in the active region (i.e., $\tau_i \cdot \dot{q}_i > 0$), the brake control torque τ_c should be set to zero since it is unachievable by the brake. Taking this control feature into account, the brake control torque can be obtained by adopting the Karnopp's stick-slip model [9] as follows:

Slip mode ($\dot{q} \neq 0$)

$$\tau_c = \begin{cases} -\text{sgn}(\dot{q})|\tau_d| & \text{if } \text{sgn}(\dot{q}) \neq \text{sgn}(\tau_d) \\ 0 & \text{else} \end{cases}, \quad (3a)$$

Stick mode ($\dot{q} = 0$)

$$\tau_c = \begin{cases} -\tau_h & \text{if } \text{sgn}(\tau_h) \neq \text{sgn}(\tau_d) \\ 0 & \text{else} \end{cases}, \quad (3b)$$

where τ_h is the hand torque input to the device by a human operator and $\dot{q}$ is the joint velocity. The control torque is created in the opposite direction to either its shaft rotation in (3a) or the external hand torque acting on its shaft in (3b). Note that if the desired torque has the same sign as the joint velocity or hand torque, the brake should be released (i.e., $\tau_c = 0$) to avoid producing brake torque, which is against the user's intention. In this paper (3) will be termed as the passive constraint.

In the passive constraint (3), the quantities τ_h and $\dot{q}$ are used to determine the sign of the control torque τ_c as follows:

1. $\tau_c \geq 0$ if $\dot{q} < 0$ or $\tau_h < 0$ with $\dot{q} = 0$,
2. $\tau_c \leq 0$ if $\dot{q} > 0$ or $\tau_h > 0$ with $\dot{q} = 0$.

In this case, it is assumed that $\tau_d \neq 0$ and $\tau_h \neq 0$, because $\tau_d = 0$ on the slip mode and $\tau_h = 0$ on the stick mode is set τ_c to zero. ($\tau_d = 0$ means that there is no need for force display and $\tau_h = 0$ in the stick mode means staying at the current position.) Likewise, a set of possible brake torques for a multi-DOF mechanism can be considered. From all possible combinations of joint velocities and hand torque inputs, it is observed in a 2 DOF mechanism that control torques can be represented by 4 regions as shown in Fig. 2(a), regardless of whether the joints are in either the slip mode or the stick mode.

A set of passive FMEs can be drawn by mapping τ_c in the joint space into the end-effector force $\mathbf{F}_c$ in the task space using the Jacobian mapping of (2). Thus, each region in Fig. 2(a) is mapped into each corresponding passive FME illustrated in Fig. 2(b), which represents a set of passive FMEs. Each passive FME is delimited by four reference forces $\mathbf{R}_{1+}$, $\mathbf{R}_{1-}$, $\mathbf{R}_{2+}$, and $\mathbf{R}_{2-}$, where $\mathbf{R}_i$ denotes the end-effector force when only brake i is applied (i.e., $\tau_{ci} \neq 0$) with the other brakes released. For example, if $\tau_{c1} > 0$ (or $\tau_{c1} < 0$) with $\tau_{c2} = 0$, then force $\mathbf{R}_{1+}$ (or $\mathbf{R}_{1-}$) is generated. Likewise, $\mathbf{R}_{2+}$ (or $\mathbf{R}_{2-}$) is generated for $\tau_{c2} > 0$ (or $\tau_{c2} < 0$) with $\tau_{c1} = 0$. Since the reference forces determine the range of directions in which a force can be generated for a given end-effector velocity, their computation is the first step to the analysis of the passive FME. From (2), the force created at the end-effector can be computed by

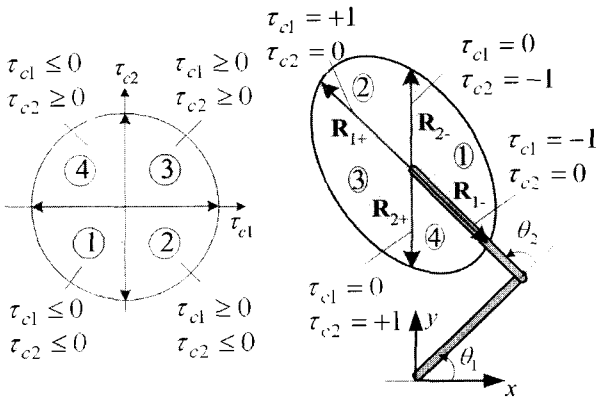

(a) Joint space (b) Task space

Fig. 2. A set of passive FMEs. ($\theta_1 = 45°$, $\theta_2 = 90°$, $l_1 = l_2 = l$)

$$\mathbf{F} = \mathbf{J}(\mathbf{q})^{-T}\tau. \quad (4)$$

In the case of the 2-link manipulator, $\mathbf{J}^{-T}$ is given by

$$\mathbf{J}^{-T} = \frac{1}{l_1 l_2 s_2}\begin{bmatrix} l_2 c_{12} & -l_1 c_1 - l_2 c_{12} \\ l_2 s_{12} & -l_1 s_1 - l_2 s_{12} \end{bmatrix} = [\mathbf{J}_1 \mid \mathbf{J}_2] \quad (5)$$

and the reference forces can be easily computed by the following relations

$$\mathbf{R}_{i+} = \mathbf{J}_i, \mathbf{R}_{i-} = -\mathbf{J}_i, \quad (6)$$

where the subscript i denotes the joint number, and $\mathbf{J}_i$ is the ith column vector of $\mathbf{J}^{-T}$. For example, $\mathbf{R}_{1+}$ corresponds to $\tau_{c1} = 1$ and $\tau_{c2} = 0$ and $\mathbf{R}_{1+} = \mathbf{J}_1$. Note that the Jacobian and reference forces change as the manipulator moves.

Consider an example in Fig. 3 for detailed analysis. Suppose that the end-effector P is moving in the $-y$ direction (i.e., $\dot{\theta}_1 < 0$ and $\dot{\theta}_2 > 0$). Hence, the brakes can generate a force only in passive FME 2 (i.e., $\tau_{c1} > 0$ and $\tau_{c2} < 0$) due to the passive constraint. Note in passive FME 2 that $\tau \cdot \dot{\mathbf{q}} = \tau_{c1}\dot{\theta}_1 + \tau_{c2}\dot{\theta}_2 < 0$ in (1), since $\tau_{c1}\dot{\theta}_1 < 0$ and $\tau_{c2}\dot{\theta}_2 < 0$. Since passive FME 2 belongs to passive region I, the desired force $\mathbf{F}_{d1}$ in this region can be accurately displayed by a resultant force of $\mathbf{R}_{1+}$ and $\mathbf{R}_{2-}$. Conversely, the desired $\mathbf{F}_{d2}$ belonging to passive region II must be represented by the combined force of $\mathbf{R}_{2-}$ and $\mathbf{R}_{1-}$ in Fig. 3. However, generation of $\mathbf{R}_{1-}$ requires $\tau_{c1} < 0$, which violates the passive constraint of $\tau_{c1} \cdot \dot{\theta}_1 \leq 0$. Therefore, $\mathbf{F}_{d2}$ cannot be accurately displayed but rather approximated by the nearest available force $\mathbf{R}_{2-}$ alone, which is called *force approximation* in passive haptic devices. Finally, the desired force $\mathbf{F}_{d3}$ cannot be displayed at all since it belongs to the active region of $\mathbf{F} \cdot \mathbf{v} > 0$. In the case of

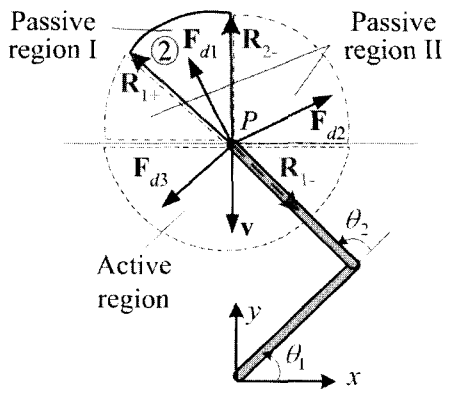

Fig. 3. Force approximation.
($\theta_1 = 45°$, $\theta_2 = 90°$, $l_1 = l_2 = l$)

passive haptic devices, consequently, there exist regions in which the desired force cannot be displayed or can be displayed only approximately and these regions can be found by the passive FME analysis.

3. UNSMOOTH DISPLAY

A wall-following operation is a good example to evaluate the performance of haptic display, in that the end-effector moves on the surface of a virtual wall. It is difficult, however, to achieve smooth and accurate movement along the surface with a passive haptic device. Actual movement of the end-effector becomes somewhat unsmooth due to force approximation as illustrated in Fig. 3. In what follows, unsmooth motion due to force approximation will be discussed in detail.

Before dealing with the passive haptic device, consider the unstable behavior of the active haptic device. The active haptic device can cause the end-effector to move toward the surface or even leave the wall surface using the active torque from the motor once it penetrates into the wall. This so-called pullback motion is beneficial to precisely representing the virtual environment (VE), but it easily leads to unstable behavior - repeated contact and non-contact with the wall – due to energy leaks such as time delay (e.g., the update period of VE) [10]. On the ideal condition in which no energy leak arises, however, an active haptic device can display the wall smoothly. If it does not possess pullback capability, smooth display can be achieved even when energy leak occurs. Smooth display on the wall-following task by a passive haptic device is expected, since a passive haptic device itself cannot produce pullback motion. However, unsmooth motion frequently occurs during the wall-following task due to energy leak as in the active device.

Time delay is mainly caused by the slow update rate of the virtual environment (VE). In an ideal situation, the end-effector should not penetrate into the wall since the wall is hard enough to prevent penetration.

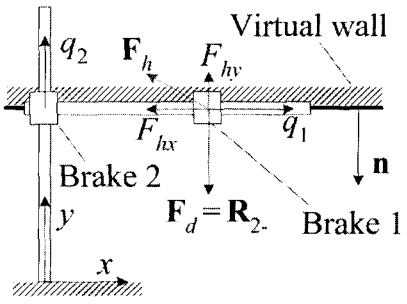

Fig. 4. XY table mechanism.

In the actual situation, however, penetration by hand force continues until it is detected at the next update time of the VE at which point it is then stopped by the brake action. This penetration can be minimized by increasing the VE update rate, but it is limited by the graphic update rate and computation of physical laws for implementation of the VE.

In the next section, we will show how a passive haptic device is capable of pullback motion. First, the case without force approximation, in which smooth display is achieved regardless of time delay, is discussed. Then pullback capability caused by force approximation is analyzed in detail.

3.1. Force display without force approximation

Consider the XY table mechanism shown in Fig. 4, where brakes 1 and 2 control the x-axis and y-axis movements independently. Assume that the surface of the wall is frictionless. $\mathbf{F}_h$ denotes a hand force input by a human operator and F_{hx} and F_{hy} are its components in the x and y axes, respectively. $\mathbf{n}$ is the surface normal vector in the $-y$ direction. Since the desired force $\mathbf{F}_d$ is exactly matched with the reference force $\mathbf{R}_{2-}$, it can be accurately displayed without force approximation using only brake 2.

Consider the motion of the end-effector along the y axis. As the penetration of the end-effector into the virtual wall increases, brake 2 also increases its braking force until achieving the fully locked level. Then the penetration depth remains at a constant value during the wall-following task on the virtual wall with brake 2 locked, until the user wishes to pull it back (i.e., the sign of F_{hy} changes). Thus, pullback motion by a brake does not occur in this case. The end-effector can smoothly move due to the free motion of joint 1 on the x-axis while maintaining the penetration depth constant. Time delay due to the slow VE update rate will not affect the performance of the haptic display in this ideal situation of the wall-following task.

3.2. Force display with force approximation

If the virtual wall in Fig. 4 is slanted, then force approximation must be performed. The forces acting on the end-effector in this case are illustrated in Fig. 5

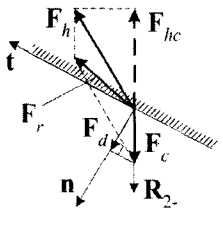

(a) Small penetration depth $|\mathbf{F}_{hc}| > |\mathbf{F}_c|$

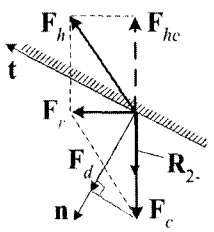

(b) Large penetration depth $|\mathbf{F}_{hc}| \leq |\mathbf{F}_c|$

Fig. 5. Forces acting on the end-effector under different penetration depths.

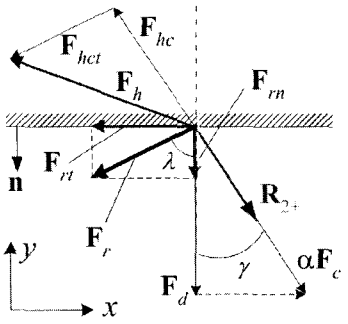

Fig. 6. Forces acting on the end-effector.

for different penetration depths resulting in diverse values of a desired force $\mathbf{F}_d$. The vectors **n** and **t** are the unit vectors normal and tangent to the virtual wall, respectively. Assume that $\mathbf{F}_d$ can be displayed only approximately by the nearest reference force $\mathbf{R}_{2-}$. Thus, a control force $\mathbf{F}_c$ activated by brake 2 is in the same direction as $\mathbf{R}_{2-}$. A hand force input, $\mathbf{F}_h$, has a component $\mathbf{F}_{hc}$ in the direction of $\mathbf{F}_c$. Note that $\mathbf{F}_h$ is assumed to be constant for easy understanding. $\mathbf{F}_r$ is a resultant force of external forces (i.e., $\mathbf{F}_h$ and $\mathbf{F}_c$), acting on the end-effector.

Upon initial contact with the virtual wall, penetration depth is very small, so $|\mathbf{F}_{hc}| > |\mathbf{F}_c|$ (i.e., case (a) in Fig. 5). Hence, the slip mode occurs at brake 2 and $\mathbf{F}_r$ has a normal component directed into the wall, thus resulting in increasing penetration. As penetration continues, at some instant, case (b) in Fig. 5 (i.e., $|\mathbf{F}_{hc}| \leq |\mathbf{F}_c|$) takes place, where brake 2 is fully locked and the stick mode is activated. In the stick mode, $|\mathbf{F}_c| = |-\mathbf{F}_{hc}|$ (see (3b)). Thus $\mathbf{F}_{hc}$ is canceled out by $\mathbf{F}_c$ and only $\mathbf{F}_r$ remains. The normal component of $\mathbf{F}_r$ in the case of (b) is directed outward, thus causing the end-effector to leave the wall surface. During the process of force approximation, the passive haptic device has pullback motion which would otherwise only be possible by the active actuator. Thus, the passive haptic device with force approximation can exhibit unsmooth (or even) motion as long as (or no) time delay exists.

4. DIRECT CONTROL

In the previous section, we observed that fullback motion is possible in the case of a passive haptic device. In this situation, the end-effector loses contact with the surface of the virtual wall, although the human operator desires to move the end-effector on the surface. Therefore, our control objective is to imitate the ideal display described in Fig. 4, since the ideal display never loses contact once the end-effector penetrates into the wall unless the human operator pulls the end-effector back off the surface. If we can make the normal component of a resultant force be zero in the case of Fig. 5(b), smooth display can be achieved regardless of time delay as shown in Fig. 4. In what follows, we will demonstrate how the normal component of a resultant force vanishes to imitate the ideal display in Fig. 4.

Fig. 6 illustrates various forces involved in representing a virtual wall. A proper brake control scheme can be found by observing the relations of these forces. If the desired force $\mathbf{F}_d$ is displayed approximately by the reference force $\mathbf{R}_{2+}$, for example, then the control force $\mathbf{F}_c$ is generated by the brake in the direction of $\mathbf{R}_{2+}$. An angle γ between $\mathbf{F}_d$ and $\mathbf{F}_c$ represents an approximation angle which is indicative of a level of force approximation. A greater approximation angle leads to poorer haptic display in a passive haptic device. The resultant $\mathbf{F}_r$ of all the forces acting on the end-effector becomes

$$\begin{aligned}\mathbf{F}_r &= \mathbf{F}_{rn} + \mathbf{F}_{rt} \\ &= \mathbf{F}_h + \alpha \mathbf{F}_c \\ &= \mathbf{F}_{hc} + \mathbf{F}_{hct} + \alpha \mathbf{F}_c ,\end{aligned} \tag{7}$$

where $\mathbf{F}_{rt}$ and $\mathbf{F}_{rn}$ are the tangent and normal components of $\mathbf{F}_r$, and α is the scale factor to be determined. (7) is applicable to both slip and stick modes. Suppose that $|\mathbf{F}_{hc}| \leq |\alpha \mathbf{F}_c|$. As mentioned above, the brake is in the stick mode ($|\alpha\mathbf{F}_c| = |-\mathbf{F}_{hc}|$). As such, $\mathbf{F}_{hc}$ is canceled out by $\mathbf{F}_c$ and only $\mathbf{F}_{hct}$ remains in $\mathbf{F}_r$. In the case of the stick mode ($|\mathbf{F}_{hc}| > |\alpha\mathbf{F}_c|$), a force in $\mathbf{F}_c$ direction can be $\mathbf{F}_{hc} + \alpha\mathbf{F}_c$. Thus, (7) holds for all cases. From the observation that unsmooth wall-following is caused by repeated contact and non-contact of the end-effector with the wall, the proposed brake control attempts to make the normal component $\mathbf{F}_{rn}$ be zero by adjustment of a brake torque. Then the end-effector becomes subject to only the tangential force along the surface, thereby leading to smooth wall-following without leaving the wall surface. In what follows, the scale factor α which makes $\mathbf{F}_{rn}$ vanish will be derived.

First, $|\mathbf{F}_{rn}|$ is computed by

$$|\mathbf{F}_{rn}| = |\mathbf{F}_r| \cos\lambda , \tag{8}$$

where λ is the angle included between $\mathbf{F}_d$ and $\mathbf{F}_r$. Since the desired force $\mathbf{F}_d$ is normal to the surface, $\mathbf{n} = \mathbf{F}_d / |\mathbf{F}_d|$, $\cos\lambda$ can be expressed by

$$\cos\lambda = \frac{\mathbf{F}_r \cdot \mathbf{F}_d}{|\mathbf{F}_r||\mathbf{F}_d|}. \tag{9}$$

Substitution of (7) and (9) into (8) yields

$$|\mathbf{F}_{rn}| = |\mathbf{F}_h + \alpha\mathbf{F}_c| \frac{(\mathbf{F}_h + \alpha\mathbf{F}_c)\cdot\mathbf{F}_d}{|\mathbf{F}_r||\mathbf{F}_d|}. \tag{10}$$

Because $\mathbf{F}_r = \mathbf{F}_h + \alpha\mathbf{F}_c \neq 0$ in general, $|\mathbf{F}_{rn}| = 0$ can be achieved when

$$(\mathbf{F}_h + \alpha\mathbf{F}_c)\cdot\mathbf{F}_d = 0. \tag{11}$$

Hence, α can be obtained by

$$\alpha = -\frac{\mathbf{F}_h \cdot \mathbf{F}_d}{\mathbf{F}_c \cdot \mathbf{F}_d}. \tag{12}$$

Let us investigate the sign of α. Only when $\mathbf{F}_h \cdot \mathbf{F}_d < 0$, the user intends to move the end-effector while maintaining it in contact with the wall; otherwise, the user intends to move the end-effector off the wall and thus force reflection is unnecessary. On the other hand, only when $\mathbf{F}_c \cdot \mathbf{F}_d > 0$, the approximation angle γ between the desired and the reference force is less than 90° and thus force approximation is possible. Consequently, $\alpha > 0$ since $\mathbf{F}_h \cdot \mathbf{F}_d < 0$ and $\mathbf{F}_c \cdot \mathbf{F}_d > 0$. Furthermore, the value of α is in the range of $0 < \alpha \leq 1$. Note that $\alpha > 1$ signifies that the brake is commanded to generate torque greater than the desired torque, which is unreasonable.

Considering that a virtual wall generally has the bilateral characteristic, it is appropriate that α should be computed by (12) while the end-effector is inside the wall but moves outwardly. The outward motion can cause unstable behavior as shown in the previous section. When the end-effector moves inwardly, brakes are firmly activated to retard the on-going penetration of the end-effector. Thus, α should be computed with (12), when $\mathbf{F}_d \cdot \mathbf{v} > 0$ (i.e., outward motion). This proposed scheme is called *direct control scheme* because the value of α can be determined directly from the passive FME. The direct controller is implemented as follows:

1. Compute the control force $\mathbf{F}_c$ depending on $\mathbf{F}_d$.
2. $$\alpha = \begin{cases} -\dfrac{\mathbf{F}_h \cdot \mathbf{F}_d}{\mathbf{F}_c \cdot \mathbf{F}_d} & \text{if } \mathbf{F}_d \cdot \mathbf{v} > 0 \\ 1 & \text{else} \end{cases}$$
3. Set $\mathbf{F}_c' = \alpha\mathbf{F}_c$
4. Generate brake torques according to $\tau_c' = \mathbf{J}^T \mathbf{F}_c'$.

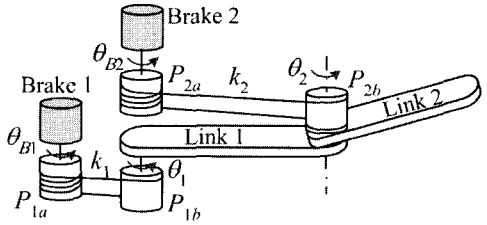

(a) Schematic.

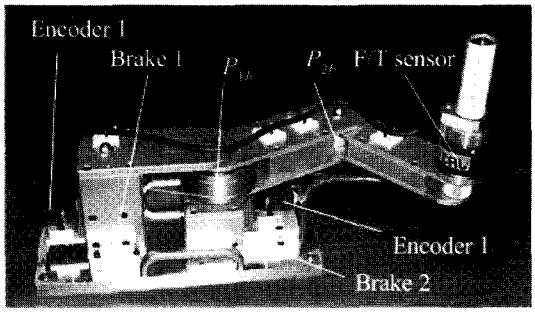

(b) Picture.

Fig. 7. Coupled tendon-drive mechanism.

Note that if $\mathbf{F}_d$ is in passive region I, then $\mathbf{F}_c$ is set to $\mathbf{F}_d$, while if in passive region II, then $\mathbf{F}_c$ is selected so that its component in the normal direction becomes $\mathbf{F}_d$.

5. EXPERIMENTS

In the previous section, the direct control method has been introduced. This will be verified through various experiments using the 2-link device equipped with 2 electric brakes.

5.1. Experimental setup

The 2-link passive haptic device equipped with 2 electric brakes shown in Fig. 7 was constructed for the experiments. The angles θ_i and θ_{Bi} represent the joint angle and the rotating angle of the brake, respectively, and k_i is the reduction ratio of the tendon-drive system. The design parameters are $k_2 = 0.4$ and $l_1 = l_2 = 0.15$m. Brake 1 (or 2), which provides a braking torque to link 1 (or 2), is mounted at the base and conveys the torque through pulleys P_{1a}-P_{1b} (or P_{2a}-P_{2b}). Placing both brakes at the base has the advantage of reducing the mass of the moving part. The FT (force/torque) sensor is mounted at the handle to measure the hand force provided by the user. The direction of hand torque is calculated from the measured hand force input by using (4). The rotational motion of each brake is sensed by the optical encoder mounted on the brake axis.

In the experiments, the brake control is conducted at a rate of 1 kHz, and the response time of the brake is about 20ms. Since the brake is capable of generating a braking torque proportional to the current input, it is controlled in an open-loop manner. The virtual wall is modeled as a spring whose constant is

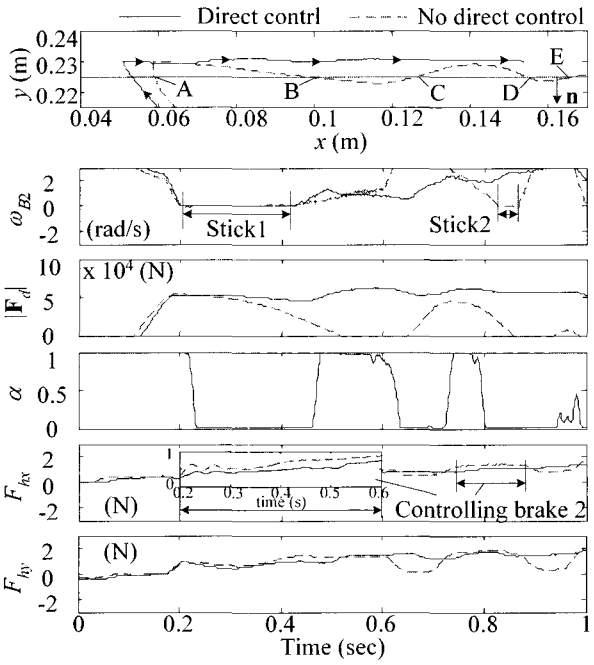

Fig. 8. Experimental results for a planar virtual wall at the update rate of 1kHz.

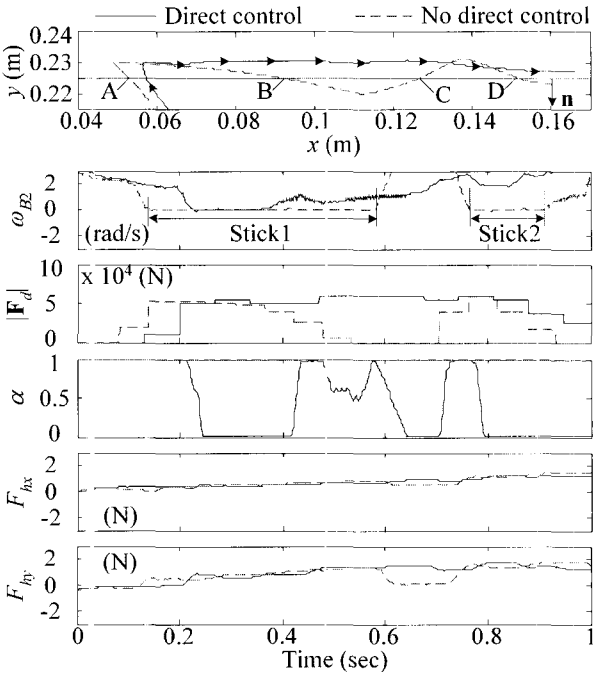

Fig. 9. Experimental results for a planar virtual wall at the update rate of 20Hz.

10^7N/m, but is assumed to possess neither damping nor friction on the surface. Thus, the direction of a desired force is the same as that of the surface normal **n**.

5.2. Experimental results

Experimental results in Figs. 8 and 9 are obtained for the plain virtual wall and shown in Fig. 6. The wall is offset 0.225m from the origin in the $+y$ direction. A hand force input is provided to move the handle mounted at the end-effector in the $+x$ direction while maintaining contact with the virtual wall.

In this situation, force approximation occurs and $\mathbf{R}_{2-}$ is used to display the virtual wall. Thus, only brake 2 is activated and brake 1 is fully released during display of the virtual wall and thus the direction of the control force coincides with that of $\mathbf{R}_{2-}$. The approximation angle γ, which is an angle between the desired force and the control force as shown in Fig. 6, increases, as the end-effector moves in the $+x$ direction. The minimum and maximum approximation angles are 3° around x = 0.06m and 33° around x = 0.17m, respectively.

The experimental results in Fig. 8 were obtained at the virtual wall update rate of 1 kHz, which is identical to that of the brake control. It is observed that excessive penetration into the wall occurs initially around x = 0.05m, although the wall stiffness is great enough to prevent such penetration (i.e., 10^7N/m). This is caused by the time delay due to the slow update rate of the virtual wall and the dynamic characteristics of each brake. It is closely related to the response time of each brake and the velocity at contact. Using brakes having a faster response time or slower velocity at contact will reduce the penetration depth.

A smooth path of the end-effector is observed after initial contact is made with direct control. The penetration depth also remains at a relatively constant value, while contact and non-contact are repeated with no direct control (i.e., points A ~ E in Fig. 8). In the velocity of brake 2 (i.e., ω_{B2}), the stick mode period to generate a very large desired force was reduced in the direct control scheme. This means that brake 2 is not completely locked during direct control. The scale factor α calculated by (12) is nearly zero to compensate for a very large desired force ($5\text{x}10^4$ N) with small hand force inputs (below 2N, F_{hy} in Fig. 8). An abrupt change in F_{hy} is greatly reduced with direct control, while that with no direct control varies relatively abruptly.

It is also noted that the tangential component of hand force F_{hx}, increases as the approximation angle γ increases. This means that a human operator feels a stronger force, which slows down the motion along the surface as γ increases. This can be easily understood by investigating the forces acting on the end-effector as shown in Fig. 6. That is, the undesired force, $|\alpha \mathbf{F}_c|\sin\gamma$, due to force approximation increases with γ, but this value is less than the force $|\mathbf{F}_c|\sin\gamma$ for no direct control because $0<\alpha \leq 1$. As a result, a human operator feels less retarding force along the surface with direct control.

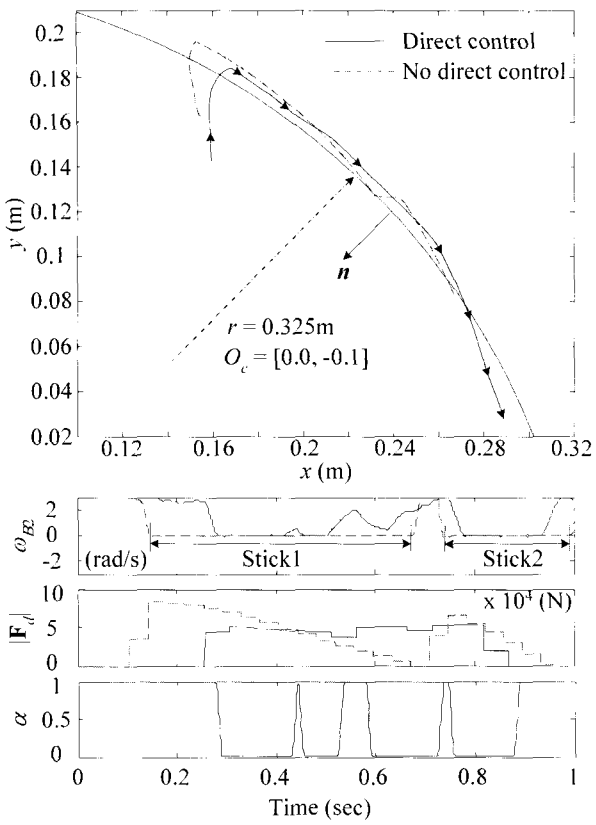

Fig. 10. Experimental results for a circular virtual wall at the update rate of 20Hz.

The experiments in Fig. 9 are conducted at the virtual wall update rate of 20Hz. Several features in Fig. 8 are similarly observed in Fig. 9. Unsmooth behavior occurs more clearly as the update rate decreases. The bouncing amplitude between contact points B and C and a change in ω_{B2} become larger than those in Fig. 8. It is observed that portions of the stick modes on ω_{B2} are increased with no direct control as the update rate decreases, while brake 2 is controlled to be in the slip mode by properly adjusting α with direct control. The hand force inputs F_{hx} and F_{hy} exhibit behaviors similar to those in Fig. 8.

A circular virtual wall whose radius is 0.325m with stiffness of 10^7N/m is implemented in the experiments shown in Fig. 10. The direction of a desired force changes as the end-effector moves along the surface. This experiment was conducted at the virtual wall update rate of 20Hz. The path for direct control demonstrates smooth behavior, while that for no direct control performs in an oscillatory manner.

6. CONCLUSIONS

In this research, a so-called direct control scheme based on the passive FME is proposed to solve the problems of force approximation and time delay in passive haptic devices. In this control scheme, the brake generates torque so that the normal component of the resultant force acting on the end-effector becomes zero. From various experiments, the following conclusions are drawn:

1. A passive haptic device with time delay can demonstrate good performance if no force approximation is made. As well, a passive haptic device with force approximation can show good performance if no time delay exists. A passive haptic device with both time delay and force approximation shows poor performance.
2. An undesired force due to force approximation retards end-effector motion along the surface. The retarding force increases as the approximation angle increases in the range of 0° to 90°. Fewer retarding forces are produced by direct control.
3. The proposed direct control scheme can improve the performance of haptic display regardless of time delay.

Since the hand force input must be precisely measured for implementation of the direct controller, a high-precision F/T sensor should be used in the experiments. It is desirable, therefore, that a control scheme that does not need such a sensor be developed for practical use.

REFERENCES

[1] J. E. Colgate, M. A. Peshkin, and W. Wannasuphoprasit, "Nonholonomic haptic display," *Proc. of the IEEE Int. Conf. on Robotics and Automation*, pp. 539-544, 1996.

[2] W. J. Book, R. Charles, H. Davis, and M. Gomes, "The concept and implementation of a passive trajectory enhancing robot," *Proc. of the ASME Dynamic Systems and Control Division*, pp.633-638, 1996.

[3] D. K. Swanson and W. J. Book, "Obstacle avoidance methods for a passive haptic display," *Proc. of the IEEE Int. Conf. on Advanced Intelligent Mechatronics*, pp.1187-1192, 2001.

[4] H. Davis and W. J. Book, "Torque control of a redundantly actuated passive manipulator," *Proc. of the American Control Conference*, pp.959-963, 1997.

[5] D. K. Swanson and W. J. Book, "Path-following control for dissipative passive haptic displays," *Proc. of 11th Symposium on Haptics*, pp. 101-108, 2003.

[6] M. Sakaguchi, J. Furusho, and N. Takesue, "Passive force display using ER brakes and its control experiments," *Proc. of Virtual Reality*, pp.7-12, 2001.

[7] C. H. Cho, M. S. Kim, and J. B. Song, "Performance analysis of a 2-link haptic device with electric brakes," *Proc. of 11th Symposium on Haptics*, pp. 47-53, 2003.

[8] T. Yoshikawa, *Foundations of Robotics: Analysis*

and Control, The MIT Press, Massachusetts, 1990.

[9] D. Karnopp, "Computer simulation of stick-slip friction in mechanical dynamic system," *ASME Journal of Dynamic Systems, Measurement, and Control*, vol. 107, pp.100-103, March 1985.

[10] B. Gillespie and M. Cutkosky., "Stable user-specific rendering of the virtual wall," *Proc. of the ASME Int. Mech. Eng. Conf. and Exp.*, DSC-Vol. 58, pp. 397-406, 1996.

Changhuyn Cho received his B.S. and M.S. degrees in Mechanical Engineering from Kyunghee University, Korea, in 1997 and 1999, respectively. He is a Doctorial Fellow in Mechanical Engineering at Korea University and KIST (Korea Institute of Science and Technology). His current research interests are design and control of robotic systems including haptic devices and actuators.

Jae-Bok Song received his B.S. and M.S. degrees in Mechanical Engineering from Seoul National University, Korea, in 1983 and 1985 respectively and a Ph.D. degree in Mechanical Engineering from MIT in 1992. He joined the faculty of the Department of Mechanical Engineering, Korea University in 1993, where he has been a Full Professor since 2002. His current research interests are robot navigation, and design and control of robotic systems including haptic devices.

Munsang Kim received his B.S. and M.S degrees in Mechanical Engineering from Seoul National University in 1980 and 1982 res-pectively and a Ph.D. in Robotics from the Technical University of Berlin, Germany in 1987. Since 1987, he has been working as a Research Scientist at the Korea Institute of Science, Korea. He has been leading the Advanced Robotics Research Center since 2000 where he became the Director of the "Intelligent Robot – The Frontier 21 Program" in Oct. 2003. His current research interests are design and control of novel mobile manipulation systems, haptic device design and control, and sensor application to intelligent robots.